

Amorphous transformation of ternary $Cu_{45}Zr_{45}Ag_{10}$ alloy under microgravity condition

Ming-Hua Su(苏明华), Fu-Ping Dai(代富平), and Ying Ruan(阮莹)
Citation: Chin. Phys. B, 2022, 31 (**9**): 098106. DOI: 10.1088/1674-1056/ac67c9
Journal homepage: http://cpb.iphy.ac.cn; http://iopscience.iop.org/cpb

What follows is a list of articles you may be interested in

Numerical simulation on dendritic growth of Al-Cu alloy under convection based on the cellular automaton lattice Boltzmann method

Kang-Wei Wang(王康伟), Meng-Wu Wu(吴孟武), Bing-Hui Tian(田冰辉), and Shou-Mei Xiong(熊守美)
Chin. Phys. B, 2022, 31 (**9**): 098105. DOI: 10.1088/1674-1056/ac7211

Multi-phase field simulation of competitive grain growth for directional solidification

Chang-Sheng Zhu(朱昶胜), Zi-Hao Gao(高梓豪), Peng Lei(雷鹏), Li Feng(冯力), and Bo-Rui Zhao(赵博睿)
Chin. Phys. B, 2022, 31 (**6**): 068102. DOI: 10.1088/1674-1056/ac4486

Phase-field modeling of faceted growth in solidification of alloys

Hui Xing(邢辉), Qi An(安琪), Xianglei Dong(董祥雷), and Yongsheng Han(韩永生)
Chin. Phys. B, 2022, 31 (**4**): 048104. DOI: 10.1088/1674-1056/ac3398

Numerical study of growth competition between twin grains during directional solidification by using multi-phase field method

Chang-Sheng Zhu(朱昶胜), Ting Wang(汪婷), Li Feng(冯力), Peng Lei(雷鹏), and Fang-Lan Ma(马芳兰)
Chin. Phys. B, 2022, 31 (**2**): 028102. DOI: 10.1088/1674-1056/ac0eed

Effects of heat transfer in a growing particle layer on microstructural evolution during solidification of colloidal suspensions

Jia-Xue You(游家学), Yun-Han Zhang(张运涵), Zhi-Jun Wang(王志军), Jin-Cheng Wang(王锦程), and Sheng-Zhong Liu(刘生忠)
Chin. Phys. B, 2021, 30 (**2**): 028103. DOI: 10.1088/1674-1056/abc168

Amorphous transformation of ternary $Cu_{45}Zr_{45}Ag_{10}$ alloy under microgravity condition

Ming-Hua Su(苏明华), Fu-Ping Dai(代富平)†, and Ying Ruan(阮莹)

School of Physical Science and Technology, Northwestern Polytechnical University, Xi'an 710072, *China*

(Received 6 March 2022; revised manuscript received 2 April 2022; accepted manuscript online 18 April 2022)

The influences of undercooling rate and cooling rate on the microstructural evolution of ternary $Cu_{45}Zr_{45}Ag_{10}$ alloy using single-roller melt spinning and drop tube are investigated. The rapidly quenched alloy ribbons achieve a homogeneous glass structure. The microstructure of the droplets transforms from the $Cu_{10}Zr_7$ dendrites plus ($Cu_{10}Zr_7$+AgZr) eutectic into $Cu_{10}Zr_7$ dendrite with the decrease of droplet diameter. As the diameter decreases to 180 μm, the $Cu_{45}Zr_{45}Ag_{10}$ alloy changes from crystal to amorphous structure, showing that the cooling rate is not the only influence factor and the undercooling play a certain role in the forming of the amorphous alloy at the same time under microgravity condition.

Keywords: Cu–Zr–Ag, rapid solidification, microgravity, glass transformation

PACS: 81.30.Fb, 81.10.Mx, 81.05.Kf **DOI:** 10.1088/1674-1056/ac67c9

1. Introduction

Rapid solidification is a liquid–solid transition process far from the equilibrium condition with the characteristics of containerless, microgravity, and high vacuum. These conditions directly affect the microstructure, phase transformation mechanism, and solidification path, further influencing the mechanical properties of the alloy, such as crystal grain refinement, metastable phase formation, solid solubility extension, even amorphous formation under this condition. Therefore, rapid solidification provides a method for preparing advanced metal materials and has attracted the extensive attention of researchers.[1–10] In the drop tube, the alloy melt falls freely at an acceleration rate of 9.8 m·s^{-2} and rapidly solidifies into droplets of different diameters. Compared with the other rapid solidification methods, the alloy obtains microgravity conditions, deep undercooling, and a high cooling rate by drop tube.[11–13] Consequently, we use a drop tube to investigate the glass transformation during the solidification.

Cu–Zr-based alloy is a kind of typical amorphous alloy system and has an extensive application in mechanical structural materials, mold materials, precision optical materials, and sports equipment due to its excellent mechanical, physical, and chemical properties.[14–17] The addition of the Ag element will improve the glass-forming ability (GFA) of the Cu–Zr–Ag alloy and exhibits excellent properties such as high strength, good ductility, and thermal stability.[18,19] The current studies of ternary Cu–Zr–Ag alloy mainly focus on the GFA, thermal stability, and liquid phase separation.[20–22] However, there are seldom researches focusing on the phase composition and microstructural characteristics of ternary Cu–Zr–Ag alloy during rapid solidification. In this work, we use the drop tube and single-roller melt spinning to study the microstructural evolution of ternary $Cu_{45}Zr_{45}Ag_{10}$ alloy. Furthermore, the possibility of metallic glass formation and the effects of cooling rate and undercooling on the amorphous transformation are also investigated.

2. Experimental methods

$Cu_{45}Zr_{45}Ag_{10}$ alloy ingots were prepared from high-purity Cu (99.999%), Zr (99.99%), and Ag (99.9999%) by arc melting under an argon atmosphere, each sample being about 2 g in weight. We performed the microgravity solidification of the alloy in a 3-m-long drop tube. The sample was placed in a Φ16 mm×150 mm quartz tube with a nozzle of Φ0.3 mm at the bottom and then melted by induction heating for several seconds. The casting temperature (1360 K) was about 200 K higher than the liquidus temperature. And then high purity argon gas was filled into the quartz tube. In the process of falling, the liquid alloy was dispersed into fine droplets with diameters of about 100 μm–1000 μm under the action of gas pressure. To make a comparative experiment, we fabricated the ribbon samples by single-roller melt spinning and the wheel speed of 40 m·s^{-1}. The sample was placed in a Φ16 mm×150 mm quartz tube with a nozzle of 1-mm size at its bottom. The casting temperature was about $T = 1360$ K and the resulting ribbons had a width of about 3 mm and a thickness of about 40 μm. The phase composition and microstructure of the samples were identified by x-ray diffraction with Cu Kα radiation (XRD, Rigaku D/max 2500 V), a scanning electron microscope (SEM, FEI Sirion Verios G4), a transmission electron microscope (TEM) (FEI Talos F200X TEM), a focused ion/electron double beam electron microscope (FIB, Helios G4 CX) and an electron dispersive spectrometer (EDS, INCA Energy 300). Thermodynamic properties were examined by differential scanning calorimetry (DSC) (Netzsch DSC 404C) at a heating rate of 10 K·min^{-1}.

†Corresponding author. E-mail: fpdai@nwpu.edu.cn

© 2022 Chinese Physical Society and IOP Publishing Ltd

3. Results and discussion

3.1. Solidification of master alloy

Figure 1(a) shows the XRD pattern of the arc melted sample. The alloy is composed of $Cu_{10}Zr_7$ phase and AgZr phase. Compared with the diffraction peaks of the AgZr phase, the strongest diffraction peak of $Cu_{10}Zr_7$ at $2\theta = 42.36°$ and the largest peak sum of $Cu_{10}Zr_7$ show that they may be the primary phase and dominant phase, respectively. To identify the solidification pathways of the $Cu_{45}Zr_{45}Ag_{10}$ alloy, we perform the DSC thermal analysis at a heating-cooling rate of 10 K·min^{-1} as shown in Fig. 1(b). The sample melts completely at 1160 K in the heating process, which is determined to be the liquidus temperature. According to the DSC cooling curve, the first exothermic peak appears at 1111 K which means that the primary $Cu_{10}Zr_7$ phase starts to solidify from the alloy melt. Then the second exothermic peak occurs at 1099 K corresponding to the solidification of the AgZr phase. The microstructure of the master alloy is shown in Figs. 1(c) and 1(d). The $Cu_{10}Zr_7$ phase grows in the form of coarse dendrites, and the lamellar ($Cu_{10}Zr_7$+AgZr) eutectic is distributed in the dendrite gap.

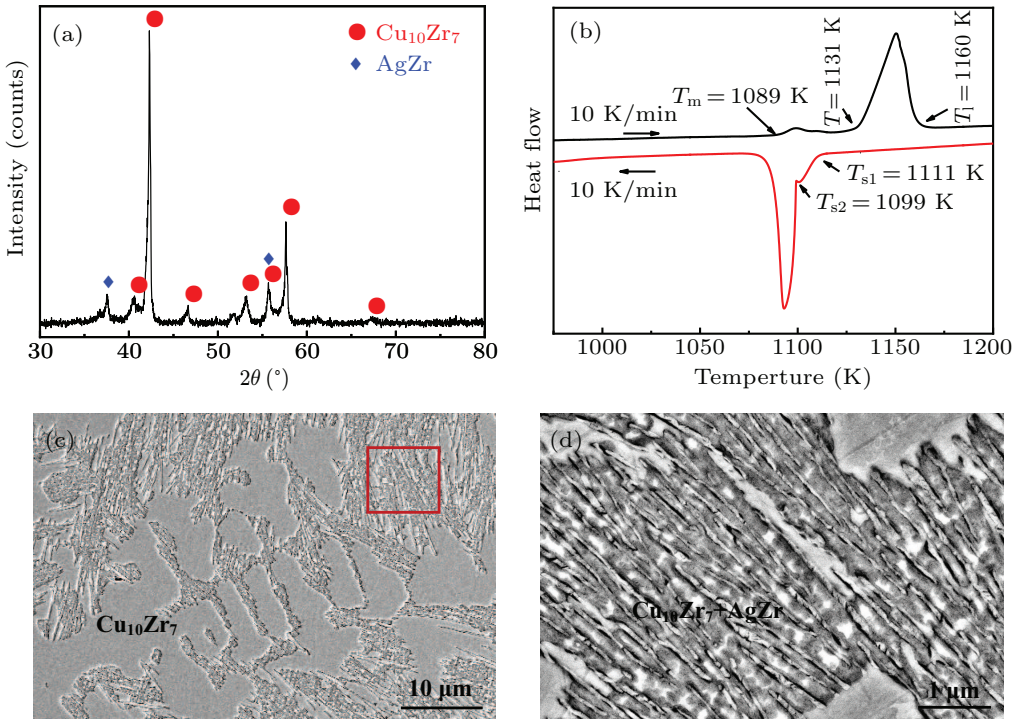


Fig. 1. (a) X-ray diffraction pattern; (b) DSC curve; (c) microstructure of alloy; (d) partial enlarged view of panel (c) of $Cu_{45}Zr_{45}Ag_{10}$ master alloy.

3.2. Solidification of alloy ribbons

To make a comparative experiment, the solidification of alloy ribbons is studied by single-roller melt spinning. Figure 2(a) shows the XRD pattern of the ribbon sample. The broad diffraction and the absence of any crystalline reflection indicate that the ribbon is in a completely amorphous state. The cooling rate of the ribbon can reach about 10^5 K·s^{-1}, indicated by calculation. When the alloy liquid is undercooled to the glass transition temperature, the alloy forms an amorphous state. We perform the DSC analysis to determine the thermal behavior of the ribbon, and the obtained results are shown in Fig. 2(b).

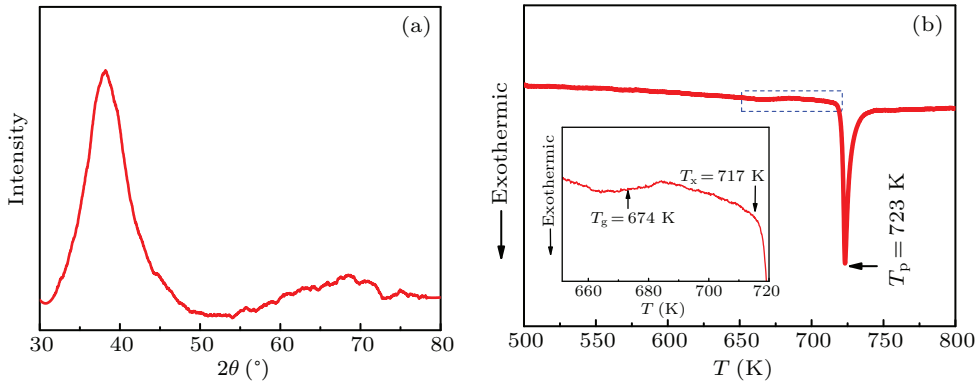


Fig. 2. (a) X-ray diffraction pattern and (b) DSC curve of rapidly quenched alloy ribbon.

With the increase in temperature, a glass transition endothermic peak and an obvious crystallization exothermic peak appear in the DSC curve successively. The starting temperatures of the two peaks are respectively designated as glass transition temperature (T_g) and crystallization temperature (T_x), and the maximum of the crystallization exothermic peak is designated as T_p. The glass transition temperature $T_g = 674$ K, crystallization temperature $T_x = 717$ K, undercooled liquid phase $\Delta T_x = 43$ K, and crystallization peak temperature $T_p = 723$ K are obtained.

3.3. Solidification of alloy droplets

3.3.1. Undercooling and cooling rate

The heat transfer inside the alloy melt will directly affect the microstructural characteristics of the droplets and it is difficult to measure the temperature variation during free fall. We use Newton's cooling model[23] to calculate the cooling rate R_c as follows:

$$R_c = \dot{T} = \frac{6}{\rho_L C_{PL} D}\left[\varepsilon\sigma\left(T^4 - T_0\right) + h\left(T - T_0\right)\right], \tag{1}$$

where ρ_L is the density of alloy droplets, C_{PL} is the specific heat, D is the diameter of alloy droplets, ε is the radiation coefficient, σ is the Stefan–Boltzmann constant, T is the ambient temperature, and h is the heat transfer coefficient. Furthermore, we calculate the undercooling ΔT of alloy droplets according to the heat transfer model proposed by Lee and Ahn[24] as follows:

$$\frac{\Psi(D)}{T_N \cdot \Delta T^2} = \ln \Phi\left(T_N, D\right), \tag{2}$$

$$\Psi(D) = \frac{16\pi\sigma_{SL}^3 T_L^2 f(D)}{3k_B\rho_L^2\Delta H^2}, \tag{3}$$

$$\Phi\left(T_N, D\right) = \frac{(\pi/6)D^3 K_V \Delta T^3 T_N^2}{\Psi(D)\dot{T}\left(3T_N - T_L\right) + \left[\kappa + 2\varepsilon\left(T_N - T_0\right)\right]\Delta T^3 T_N^3}, \tag{4}$$

$$\kappa = \frac{12k_g}{\rho_L C_{PL} D^2}, \tag{5}$$

where T_N is the nucleation temperature, $f(D)$ the heterogeneous nucleation factor, T_L the liquidus temperature, σ_{SL} the liquid–solid interface energy, k_B the Boltzmann constant, ΔH the melting enthalpy, K_V the kinetic parameter, and k_g the thermal conductivity of the gas. The calculation results obtained from Eqs. (1)–(5) are shown in Fig. 3. The related physical parameters used in the calculations are listed in Table 1. The R_c increases from 0.93×10^3 K·s^{-1} to 4.46×10^4 K·s^{-1} and ΔT increases from 42 K to 264 with the decrease of diameter.

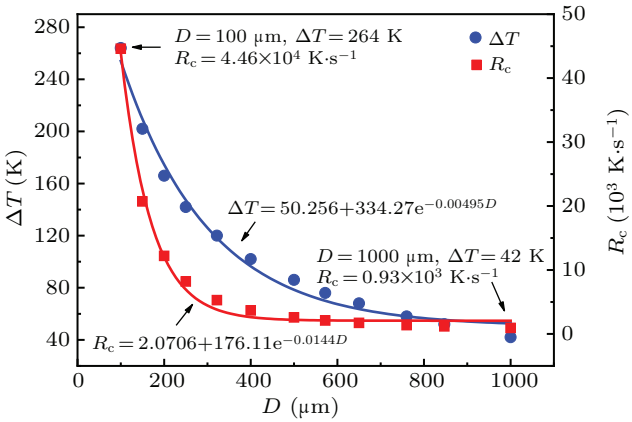


Fig. 3. Cooling rate and undercooling rate *versus* droplet diameter of ternary $Cu_{45}Zr_{45}Ag_{10}$ alloy.

Table 1. Physical parameters of $Cu_{45}Zr_{45}Ag_{10}$ alloy.[25]

Physical parameter	Value
Liquidus temperature of the alloy, T_L (K)	1160
Heat of fusion of alloy, ΔH_m (J·kg^{-1})	1.83×10^5
Density of liquid alloy, ρ_L (kg·m^{-3})	6.81×10^3
Specific heat of liquid alloy, C_{pL} (J·kg^{-1}·K^{-1})	401
Radiation coefficient, ε	0.29
S/L interfacial energy of alloy, σ_{SL} (N·m^1)	0.37
Thermal conductivity of environmental gas, λ (J·m^{-1}·s^{-1}·K^{-1})	1.77×10^{-2}
Temperature of environmental gas, T_0 (K)	300
Stefan-Boltzmann constant, σ (W·m^{-2}·K^{-4})	5.67×10^{-8}
Boltzmann constant, k_B (J·K^{-1})	1.38×10^{-23}
Kinetic parameter, k_V (m^3·s^{-1})	10^{40}

3.3.2. Microstructural characteristics

Figure 4 shows the morphologies of the alloy droplets with different diameters. For $D = 850$ μm, the primary $Cu_{10}Zr_7$ phase nucleates directly from the melt as a dendrite structure, and the ($Cu_{10}Zr_7$+AgZr) eutectic phase is distributed around dendrites (Fig. 4(a)). The cooling rate is $R_c = 1.18\times10^3$ K·s^{-1}, and the undercooling is $\Delta T = 52$ K. The alloy droplets radiate heat from the inside to the environment, and the sample surface is preferentially cooled. Thus the primary $Cu_{10}Zr_7$ dendrites first nucleate on the surface and then grow inward. Figure 4(b) shows the solidification structure of alloy droplet with a diameter of $D = 570$ μm. With the decrease in diameter, the coarse dendrites are broken and the grains are refined. The cooling rate R_c of alloy droplets reaches 2.09×10^3 K/s and the undercooling is $\Delta T = 76$ K. As the diameter decreases to $D = 320$ μm, the undercooling degree of alloy droplets is as high as $\Delta T = 120$ K, and the cooling rate reaches $R_c = 5.28\times10^3$ K·s^{-1} (Fig. 4(c)). A comparison of the sample with diameter $D = 850$ μm with that with diameter $D = 570$ μm shows that the former has larger undercooling and cooling rate. During solidification, the primary $Cu_{10}Zr_7$ phase first precipitates from the alloy, and then rapidly nucleates and grows up. There is not enough time for eutectic reaction due to the high cooling rate and undercooling. Therefore,

the eutectic reaction does not yet occur, and the alloy droplets are solidified. So, only the primary $Cu_{10}Zr_7$ phase is observed in the solidified microstructure, but no eutectic phase is observed (Fig. 4(d)).

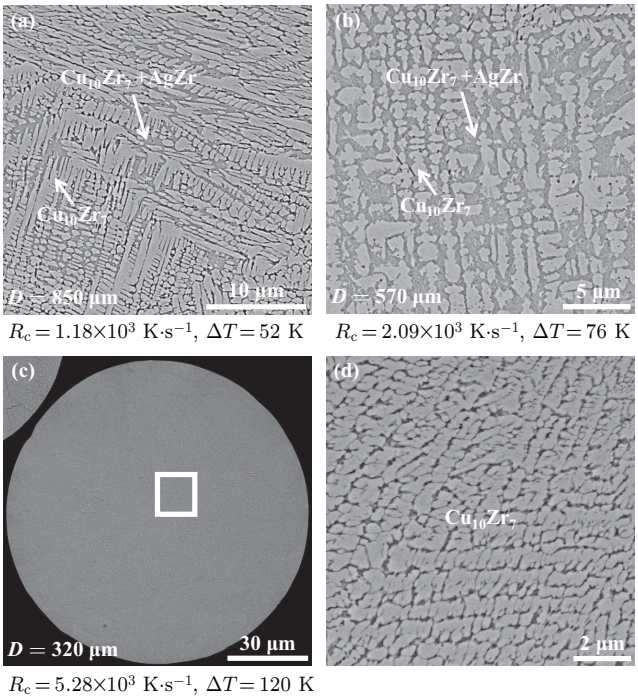


Fig. 4. Solidified microstructure of $Cu_{45}Zr_{45}Ag_{10}$ alloy droplets with diameter $D = 850$ μm (a), 570 μm (b), and 320 (c) μm, (d) magnified part of panel (c).

The $Cu_{45}Zr_{45}Ag_{10}$ is an amorphous component, and it is reported that in most of researches of this system the traditional quenching method was used.[26,27] Under the microgravity condition, the alloy droplets are in a high vacuum environment and do not contact the container wall during the falling, thus obtaining a high cooling rate and deep undercooling. Therefore, to explore whether the amorphous transformation of the $Cu_{45}Zr_{45}Ag_{10}$ alloy can take place in the drop tube, we further analyze the alloy droplets with a diameter of $D =$ 180 μm. In the case of the droplets with $D = 180$ μm, the cooling rate and undercooling reach 1.48×10^4 K·s^{-1} and 178 K respectively. The cooling rate of alloy ribbon under single-roller quenching condition can reach about 10^5 K·s^{-1}. We analyze the microstructural characteristics of the $D = 180$ μm alloy droplets by TEM and focused ion/electron double beam electron microscope (FIB). As shown in Figs. 5(a) and 5(b), a small sample is cut from the alloy droplet, where the thickness of the thin area of the sample is about 53.96 nm. The atoms are randomly arranged without any ordered structure, and the selective diffraction pattern shows wide and dispersed halo rings, the pattern which is a typical amorphous diffraction pattern as shown in Figs. 5(c) and 5(d). Therefore, the alloy droplets with $D = 180$ μm can be determined to have an amorphous structure, and the EDS analysis give the evidence of a homogeneous glassy structure in Fig. 6. Figure 7 shows the microstructural evolution of the alloy.

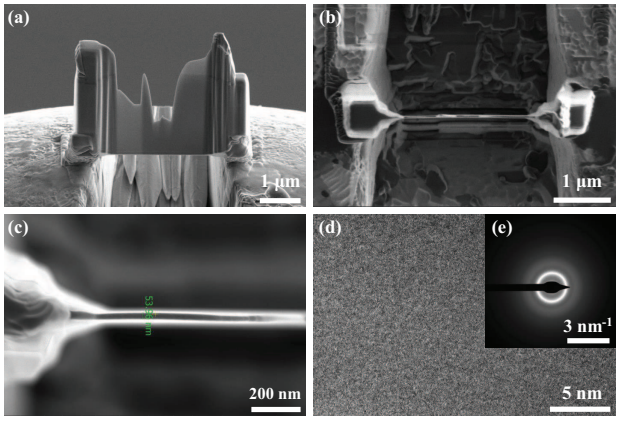


Fig. 5. Preparing [(a)–(c)] TEM and FIB sample of solidified microstructure of $Cu_{45}Zr_{45}Ag_{10}$ alloy droplet with a diameter of 180 μm; (d) high-resolution TEM image; (e) selected area electron diffraction map.

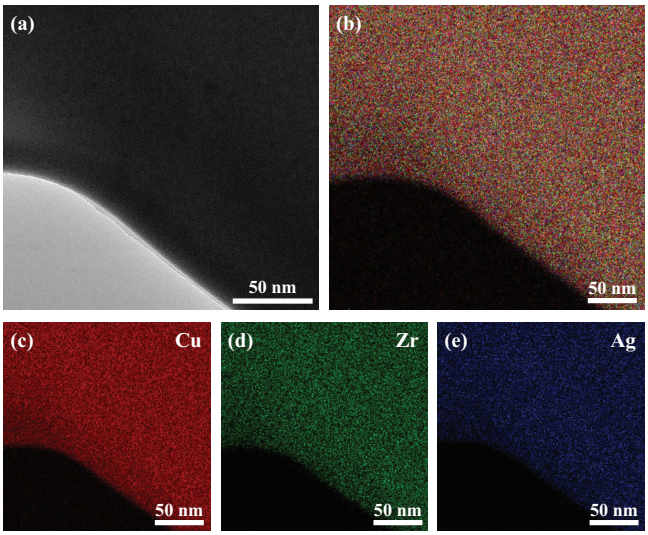


Fig. 6. EDS analyses of 180-μm-diameter $Cu_{45}Zr_{45}Ag_{10}$ alloy droplets.

To sum up, with the decrease in diameter, the undercooling and cooling rate increase, and the ternary $Cu_{45}Zr_{45}Ag_{10}$ alloy realizes the transformation from crystal into an amorphous structure under the microgravity condition. According to the calculation results, the cooling rate and the undercooling degree of alloy ribbon under single-roller quenching conditions are about 10^5 K·s^{-1} and 43 K, respectively. And the cooling rate and the undercooling degree of the droplets with $D = 180$ μm are about 10^4 K·s^{-1} and 178 K, respectively. By comparison, we find that the cooling rate of the droplets with $D = 180$ μm is smaller than that of the alloy ribbon, but the undercooling is greater. Under the condition of a low cooling rate and a high undercooling degree, the alloy droplets can still undergo amorphous transformation. Therefore, it is reasonable to believe that undercooling also plays an important role in the amorphous transformation of the alloy through comparative experiments.

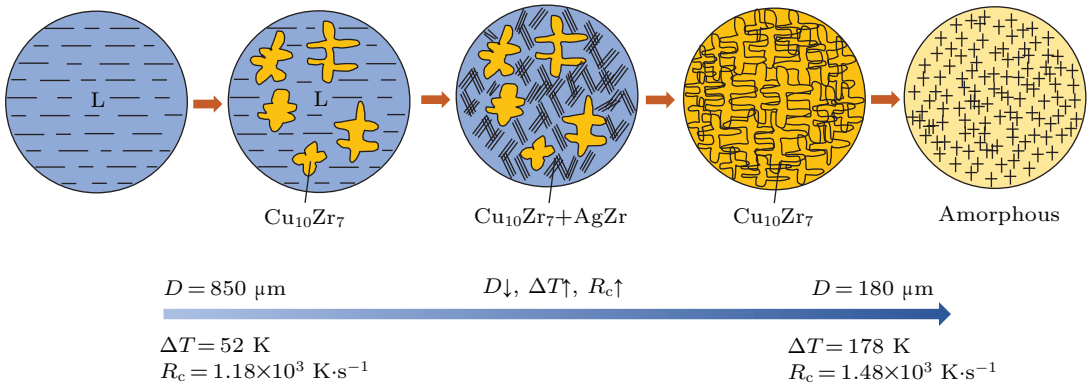


Fig. 7. Microstructural evolution of $Cu_{45}Zr_{45}Ag_{10}$ alloy droplet.

4. Conclusions

In conclusion, the microstructural evolution of the ternary $Cu_{45}Zr_{45}Ag_{10}$ alloy is investigated by the drop tube and single-roller melt spinning. The characteristic temperatures of the ternary $Cu_{45}Zr_{45}Ag_{10}$ alloy are confirmed, which are the glass transition temperature $T_g = 674$ K, crystallization temperature $T_x = 717$ K, supercooled liquid phase $\Delta T_x = 43$ K, and crystallization peak temperature $T_p = 723$ K. The alloy ribbons are completely amorphous. But the droplets during the free-falling present different crystalline states. As the droplet diameter decreases from 850 μm to 180 μm, the cooling rate and undercooling reach 1.48×10^4 K·s^{-1} and 178 K respectively. The microstructure of the droplet transforms from the mixture of primary $Cu_{10}Zr_7$ dendrites and ($Cu_{10}Zr_7$+AgZr) binary eutectic into $Cu_{10}Zr_7$ dendrites, eventually into a homogeneous metallic glass. Through comparative study, we find that under the condition of low cooling rate and high undercooling, the alloy droplets can still undergo amorphous transformation. Therefore, undercooling also plays an important role in the amorphous transformation of the alloy.

Acknowledgements

The authors would like to thank Prof. Wei B of the Key Laboratory of Space Materials Science and Technology for his support. We also thank Chen F C and Si Y F for their help in the experiment.

Project supported by the National Natural Science Foundation of China (Grant Nos. 51671161, u1806219, and 52088101) and the Natural Science Foundation Research Project of Shanxi Province, China (Grant No. 2020JZ-08).

References

[1] Lavernia E J and Srivatsan T S 2010 *J. Mater. Sci.* **45** 287
[2] Dai F P, Wu Y H, Wang W L and Wei B 2018 *Metall. Mater. Trans. A* **49A** 5478
[3] Haque N Cochrane R F and Mullis A M 2016 *Intermetallics* **76** 70
[4] Clopet C R, Cochrane R F and Mullis A M 2013 *Appl. Phys. Lett.* **102** 031906
[5] Zhou X, Liu Z W, Yu H Y, Zhang H and Zhang G Q 2020 *Physica B* **599** 412549
[6] Xu S S, Wu W H, Chang J, S S and Wei B 2022 *Metall. Mater. Trans. A* **53A** 762
[7] Zhang Y K, Zhu J, Li S, Wang J and Ren A M 2022 *J. Mater. Sci. & Tech.* **102** 66
[8] Yamauchi I and Kawamura H 2004 *J. Alloys Compd.* **370** 137
[9] Kim Y W 2008 *J. Mater. Sci. Technol.* **24** 89
[10] Kim Y W 2012 *Mater. Res. Bull.* **47** 2956
[11] Chen F C, Dai F P, Yang X Y, Ruan Y and Wei B 2020 *Chin. Phys. B* **29** 066401
[12] Cochrane R F, Evans P V and Greer A L 1988 *Mater. Sci. Eng.* **98** 799
[13] Ruan Y, Wang Q Q, Chang S Y and Wei B 2017 *Acta Mater.* **141** 456
[14] Hua H Y, Tian Y Z, Yu H W, Ling G P, Li S, Jiang M, Li H X and Qin G W 2022 *Mater. Lett.* **315** 131937
[15] Wang Q, Liu C T, Yang Y, Liu J B, Dong Y D and Lu J 2014 *Sci. Rep.* **4** 4648
[16] Calvayrac Y, Chevalier J P, Harmelin M, Quivy A and Bigot J 1983 *Phil. Mag. B* **48** 323
[17] Zhang Q, Zhang W and Inoue A 2006 *Scr. Mater.* **55** 711
[18] Duan G, Blauwe K, Lind M L, Schramm J P and Johnson W L 2008 *Scr. Mater.* **58** 159
[19] Zhang W, Jia F, Zhang Q S and Inoue A 2007 *Mater. Sci. Eng. A* **459** 330
[20] Song K K, Gargarella P, Pauly S, Ma G Z, Kuhn U and Eckert J 2012 *J. Appl. Phys.* **112** 063503
[21] Song K K, Pauly S, Zhang Y, Sun B A, He J, Ma G Z, Kühn U and Eckert J 2013 *Mater. Sci. Eng. A* **559** 711
[22] Barekar N, Gargarella P, Song K K, Kühn U and Eckert J 2011 *J. Mater. Res.* **26** 1702
[23] Levi C G and Mehrabian R 1982 *Metall. Mater. Trans. A* **13** 221
[24] Lee E S and Ahn S 1994 *Acta Metall. Mater.* **42** 3231
[25] Gale W F and Totemeir T C 2003 *Smithells Metals Reference Book*, 8th edn. (Burlington: Elsevier Butterworth-Heinemann) p. 8-1
[26] Inoue A and Zhang W 2006 *J. Mater. Res.* **21** 234
[27] Louzguine-Luzgin D V, Xie G, Zhang W and Inoue A 2007 *Mater. Sci. Eng. A* **465** 146